PC7 and the related proteases Furin and Pace4 regulate E-cadherin function during blastocyst formation

Sylvain Bessonnard,* Daniel Mesnard,* and Daniel B. Constam

Swiss Federal Institute of Technology in Lausanne, School of Life Sciences, Swiss Institute for Experimental Cancer Research, 1015 Lausanne, Switzerland

The first cell differentiation in mammalian embryos segregates polarized trophectoderm cells from an apolar inner cell mass (ICM). This lineage decision is specified in compacted morulae by cell polarization and adhesion acting on the Yes-associated protein in the Hippo signaling pathway, but the regulatory mechanisms are unclear. We show that morula compaction and ICM formation depend on PC7 and the related proprotein convertases (PCs) Furin and Pace4 and that these proteases jointly regulate cell–cell adhesion mediated by E-cadherin processing. We also mapped the spatiotemporal activity profiles of these proteases by live imaging of a transgenic reporter substrate in wild-type and PC mutant embryos. Differential inhibition by a common inhibitor revealed that all three PCs are active in inner and outer cells, but in partially nonoverlapping compartments. E-cadherin processing by multiple PCs emerges as a novel mechanism to modulate cell–cell adhesion and fate allocation.

Introduction

Early development from fertilization until the blastocyst stage in eutherian mammals is devoted to segregating a pluripotent inner cell mass (ICM) from the trophectoderm (TE) that enables attachment and survival in the mother. Differentiation of the ICM and the TE is initiated during the late eight-cell stage when individual blastomeres enlarge their cell–cell contact areas in a process termed compaction and begin to assemble junctional complexes in a polarized epithelial layer. Two subsequent rounds of symmetric or asymmetric divisions generate two identical daughters or one that is polar and one that is apolar, respectively (Handyside, 1980; Ziomek and Johnson, 1980; Johnson and Ziomek, 1981). Cultured apolar cells can become engulfed by the basolateral membrane of polarized cells, indicating that apical surfaces are less adhesive (Johnson and Ziomek, 1983; Dietrich and Hiiragi, 2007). Only apical membranes accumulate complexes of polarity proteins and atypical PKC (aPKC), and cells depleted of aPKC assume an inside position (Pauken and Capco, 2000; Plusa et al., 2005). It is possible, therefore, that cell positions are specified by asymmetric membrane inheritance. It was also reported that fates correlate with the angle of cell division (Bischoff et al., 2008). Other investigators concluded that only the most extreme symmetric divisions reliably predict outer fate (McDole et al., 2011) and that aPKC in reality promotes symmetric rather than asymmetric divisions by alleviating cortical tension and flattening cell shapes along the embryo surface (Dard et al., 2009). Accordingly, ICM fate may depend on uniform cell–cell contacts to block cell polarization and flattening (Hillman et al., 1972; Johnson and Ziomek, 1983). However, the precise mechanism specifying lineage differentiation remains unclear.

Dividing blastomeres in compacted morulae can still change positions: Inner cells occasionally rise to the surface to either assume an outer fate or quickly return to ICM, and some cells on the outside sink inside as late as during cavitation (Fleming, 1987; Yamanaka et al., 2010; McDole et al., 2011). Only the most surface-exposed mother cells in transition to the 16-cell stage give rise exclusively to outer cells, and they do so even if one daughter initially resides inside after asymmetric division (Watanabe et al., 2014). Lineage allocation, therefore, may not correlate with momentary cell positioning or polarization, but with the overall history of relative changes in cell–cell contacts.

Molecular differences among individual blastomeres already emerge before compaction. Increased DNA binding and distinct kinetics of the pluripotency determinant Oct4 and differential histone 3 arginine methylation may predict the fate of inner cells (Torres-Padilla et al., 2007; Plachta et al., 2011; Burton et al., 2013). All blastomeres initially also coexpress variable amounts of the TE lineage marker Cdx2 (Dietrich and Hiiragi, 2007; Ralston and Rossant, 2008). Unlike Oct4 kinetics, Cdx2 levels do not predict cell fate (Dietrich and Hiiragi, 2007). However, up-regulation of Cdx2 in outer cells is required to switch off *Oct4* expression in TE after

*S. Bessonnard and D. Mesnard contributed equally to this paper.

Correspondence to Daniel B. Constam: daniel.constam@epfl.ch

Sylvain Bessonnard's present address is Institut Pasteur, Centre National de la Recherche Scientifique URA 2578, Génétique Fonctionnelle de la Souris, 75724 Paris, France.

Abbreviations used in this paper: aPKC, atypical PKC; CLIP, cell-linked indicator of proteolysis; CMK, chloromethylketone; DKO, double knockout; eCFP, enhanced CFP; ES, embryonic stem; ICM, inner cell mass; PC, proprotein convertase; qRT-PCR, quantitative RT-PCR; ROI, region of interest; TE, trophectoderm; TKO, triple knockout; YAP, Yes-associated protein.

The Rockefeller University Press $30.00
J. Cell Biol. Vol. 210 No. 7 1185–1197
www.jcb.org/cgi/doi/10.1083/jcb.201503042

compaction (Strumpf et al., 2005) and to assemble tight junctions and boost mitochondrial activity (Ralston and Rossant, 2008; Wu et al., 2010).

Morula compaction, normal lineage segregation of inner and outer cells, and the regulation of *Cdx2* expression critically depend on the cell–cell adhesion molecule E-cadherin (Stephenson et al., 2012). Until the early eight-cell stage, E-cadherin localizes on all cell surfaces, but thereafter becomes restricted to cell contacts during compaction (Vestweber et al., 1987). Meanwhile, apical surfaces of outer cells lacking contacts accrue aPKC, which enables the formation of tight junctions during TE epithelialization (Eckert et al., 2004, 2005). Mutant morula devoid of E-cadherin fail to compact and show ectopic aPKC membrane staining and elevated Cdx2 protein levels at the expense of Oct4 expression even in inner cells (Stephenson et al., 2010). In keeping with a role in ICM formation, depletion of E-cadherin by RNAi in only a subset of cells directs their progeny to the outside. In contrast, the progeny of blastomeres injected with dominant-negative mutant aPKC are diverted to ICM (Plusa et al., 2005). These observations established that E-cadherin and aPKC promote inner and outer fates, respectively, and that aPKC activity is limited by E-cadherin. E-cadherin is stabilized at cell–cell contacts by calcium-dependent homotypic interactions of its extracellular domain (Pey et al., 1998; Brasch et al., 2012). In inner cells that are surrounded by neighbors, E-cadherin thus accumulates circumferentially in adherens junctions that recruit the actin-binding proteins Nf2/Merlin and Angiomotin, thereby inducing the phosphorylation and cytoplasmic retention of Yes-associated protein (YAP) by Lats1/2 kinases. In contrast, polarization of nonadherent surfaces by activated aPKC sequesters Angiomotin and Lats1/2 beneath apical membranes (Cockburn et al., 2013; Hirate et al., 2013; Leung and Zernicka-Goetz, 2013; Anani et al., 2014). Because of the resulting inhibition of Lats1/2 signaling, polarized outer cells can translocate YAP to the nucleus, where it binds the transcriptional activator Tead4 to induce *Cdx2* (Nishioka et al., 2008, 2009).

E-cadherin is synthesized as a precursor comprising an N-terminal prodomain, five cadherin repeats, a transmembrane, and a cytoplasmic domain. Prodomain cleavage enables calcium-dependent homotypic interactions among E-cadherin extracellular domains (Ozawa and Kemler, 1990). Cleavage is enhanced in insect cells that overexpress the endoprotease Furin in the trans-Golgi/endosome network and in the extracellular space (Bosshart et al., 1994; Molloy et al., 1994; Posthaus et al., 1998; Denault et al., 2002). However, E-cadherin processing was not inhibited in *FURIN*-deficient LoVo colon carcinoma cells and only reduced by <50% in breast cancer cells treated with 200-µM decanoyl-Arg-Val-Lys-Arg-chloromethylketone (CMK; Posthaus et al., 1998; Geng et al., 2012), a potent and membrane-permeable inhibitor of all proprotein convertases (PCs; Garten et al., 1994; Jean et al., 1998). It therefore remained unclear which of these proteases, if any, mediate E-cadherin processing.

Furin, PCSK5, PACE4 (also known as PCKS6/SPC4), and PC7 (PCSK7) all cleave secreted precursor proteins that contain the minimal recognition motif RXXR (Seidah and Prat, 2012). Furin and Pace4 activate TGF-β signals mediated by Nodal to specify the fate of progenitor cells in the developing mouse epiblast (Beck et al., 2002; Mesnard et al., 2011). In *Xenopus laevis* embryos, knockdown of PC7 suppresses eye development (Senturker et al., 2012), and a PC7-like activity can cleave pro-BMP4 during gastrulation (Nelsen and Christian, 2009). However, a role for PC7 in the mouse embryo is elusive. To identify novel functions of PCs, we developed the cell-linked indicator of proteolysis (CLIP) as a transgenic reporter substrate (Mesnard and Constam, 2010). In CLIP, a PC-cleavable linker connects secreted enhanced CFP (eCFP) to citrine that is targeted to the cell surface by a glycosyl-inositol phosphate anchor. Live imaging of CFP/YFP fluorescence ratios of CLIP and a comparison with an uncleavable mutant control (CLIPm) revealed that combined zygotic deletion of *Furin* and *Pace4* inhibited CLIP processing already at the blastocyst stage by >80%. Because development did not arrest until after embryonic day (E) 5.5 (Mesnard and Constam, 2010), we asked whether the lack of *Furin* and *Pace4* during the earliest stages of development is compensated for by yet another PC family member. Our results unmask combinatorial roles of *Furin*, *PC7*, and *Pace4* in jointly regulating E-cadherin precursor processing and functionality in vitro and during morula compaction. In addition, detailed spatiotemporal mapping of PC activities in developing blastocysts revealed striking differences in their relative distribution and sensitivity toward the widely used pharmacological PC inhibitor CMK.

Results

Overlapping Furin and PC7 activities regulate aPKC-ξ localization and morula compaction

To evaluate a role for PC7, exons 3–7 encoding the translational start site, the pro region, and the catalytic domain were deleted by homologous recombination in embryonic stem (ES) cells (Fig. S1). Progeny of germline chimeras obtained from two independently targeted ES cell clones gave rise to fertile homozygous mutants at Mendelian frequency. No overt abnormalities could be identified, suggesting that PC7 is not essential under the conditions examined. To uncover overlapping functions of Furin and PC7 during early embryogenesis, we intercrossed $Furin^{+/-};PC7^{-/-}$ mice in an outbred NMRI genetic background. Analysis of progeny at E7.5 revealed 18% of empty decidua and <3% $Furin^{-/-};PC7^{-/-}$ double knockout (DKO) embryos (Fig. 1 A). Moreover, despite normal Mendelian ratios at E3.5, preimplantation embryos failed to hatch from the zona pellucida and were morphologically abnormal. To determine why $Furin^{-/-};PC7^{-/-}$ mutants might arrest development, embryos were collected at E2.5 and cultured until blastocyst stages (E3.5–4.0), followed by immunofluorescence staining of the cell polarity markers aPKC-ξ and E-cadherin and of tight junctions (ZO-1). Quantification of aPKC-ξ confirmed that it is enriched at the apical membrane of TE cells, whereas E-cadherin normally marks the basolateral side of TE and cell–cell contacts between ICM cells (Fig. 1, B and C; and Fig. S2 A; Vestweber et al., 1987; Pauken and Capco, 2000; Plusa et al., 2005). In DKO mutant blastocysts, aPKC-ξ staining increased at contacts between ICM cells expressing E-cadherin and on the basolateral side of one to four TE cells lacking contact with neighbors as determined by z-stack imaging (Fig. 1, B and C). A similar defect was observed in freshly flushed embryos (Fig. S2 B). Furthermore, even though all DKO mutants initiated blastocoel formation, this process was severely impaired both at

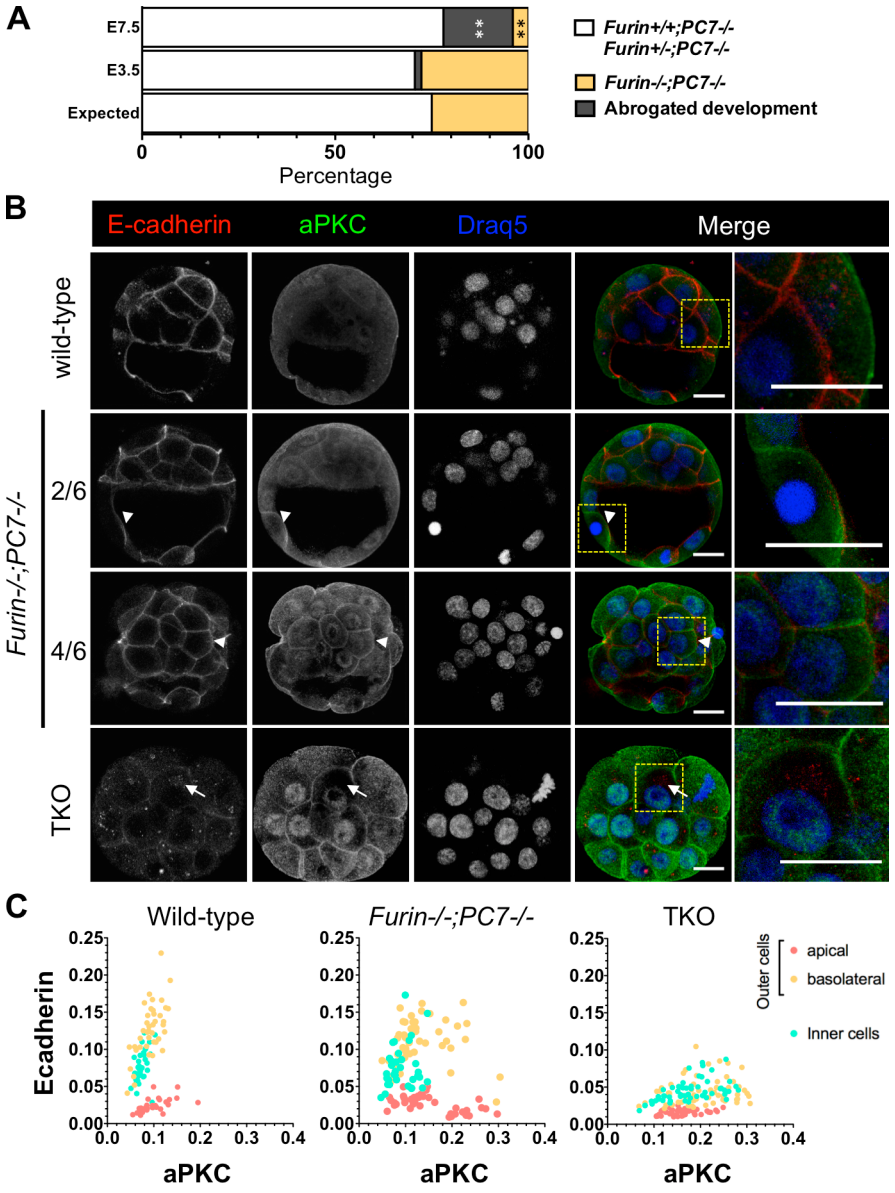

Figure 1. **Impaired cell polarity and morula compaction in *Furin*$^{-/-}$;*PC7*$^{-/-}$ and DKO and partial rescue of E-cadherin localization by Pace4.** (A) Expected Mendelian ratio and observed frequency of *Furin;PC7* double mutants at E3.5 and E7.5 after crossing with *Furin*$^{+/-}$;*PC7*$^{-/-}$ mice (**, $P < 0.01$; χ^2 test). (B) aPKC-ξ, E-cadherin, and Draq5 immunolocalization in the wild type ($n = 8$), *Furin;PC7* double mutants ($n = 6$), and *Furin;PC7;Pace4* TKO ($n = 5$), which were cultured from E2.5 until E3.5. Arrowheads indicate ectopic aPKC-ξ expression, and arrows indicate E-cadherin accumulating in the cytoplasm. Images correspond to z projections of five successive z stacks. (C) aPKC/E-cadherin quantification at the membrane of inner cells (green) and on apical (red) and basolateral (yellow) membranes of outer cells. $n = 5$ embryos per genotype. Bars, 20 µm.

E3.5 ($n = 4/6$) and after extended culture until E4.0 (Fig. 1 B, Fig. S2 C, and Table S1; $n = 4/4$), likely as a result of mislocalization of tight junctions (Fig. S2 D; $n = 5/5$). We conclude that combined loss of *Furin* and *PC7* perturbs cell polarization and compaction at the morula stage and the development of a fully expanded blastocoel cavity.

E-cadherin localization and blastocoel formation in *Furin;PC7* DKO embryos are partially rescued by Pace4

To determine whether partial rescue of blastocyst formation involves an additional PC, we analyzed triple knockout (TKO) embryos lacking *Furin*, *PC7*, and *Pace4*. Both *Pace4*$^{-/-}$ embryos and *Furin*$^{-/-}$;*Pace4*$^{-/-}$ double mutants develop normal blastocysts irrespective of genetic background (Beck et al., 2002; Mesnard and Constam, 2010). *PC7*$^{-/-}$;*Furin*$^{-/-}$;*Pace4*$^{-/-}$ TKO mutants were also found at the expected Mendelian ratios (Fig. S2 E). However, they all consisted of only loosely attached cells and failed to hatch at E3.5 or to cavitate (Fig. 1 B and Table S1; $n = 5/5$). Furthermore, double labeling of aPKC and E-cadherin revealed that E-cadherin staining at cell–cell junctions was decreased in TKO compared with DKO or wild-type embryos and relocalized to intracellular puncta, whereas aPKC-ξ was no longer confined to the embryo surface and instead accumulated ectopically along the circumference of both outer and inner cells (Fig. 1, B and C; and Fig. S2 A). aPKC and E-cadherin similarly mislocalized in freshly flushed TKO embryos (Fig. S2 B; $n = 3/3$), confirming that cell polarization is defective. Overall, these results suggest that overlapping Furin and PC7 activities are essential to correctly initiate compaction and cell polarization but that these processes are partially rescued in *Furin;PC7* DKO embryos by Pace4.

Imaging of the CLIP reporter substrate reveals sequential activation by Furin and PC7, followed by Pace4

To address whether rescue of DKO mutants temporally coincides with up-regulation of Pace4, we compared the activity profiles of individual PCs in preimplantation embryos

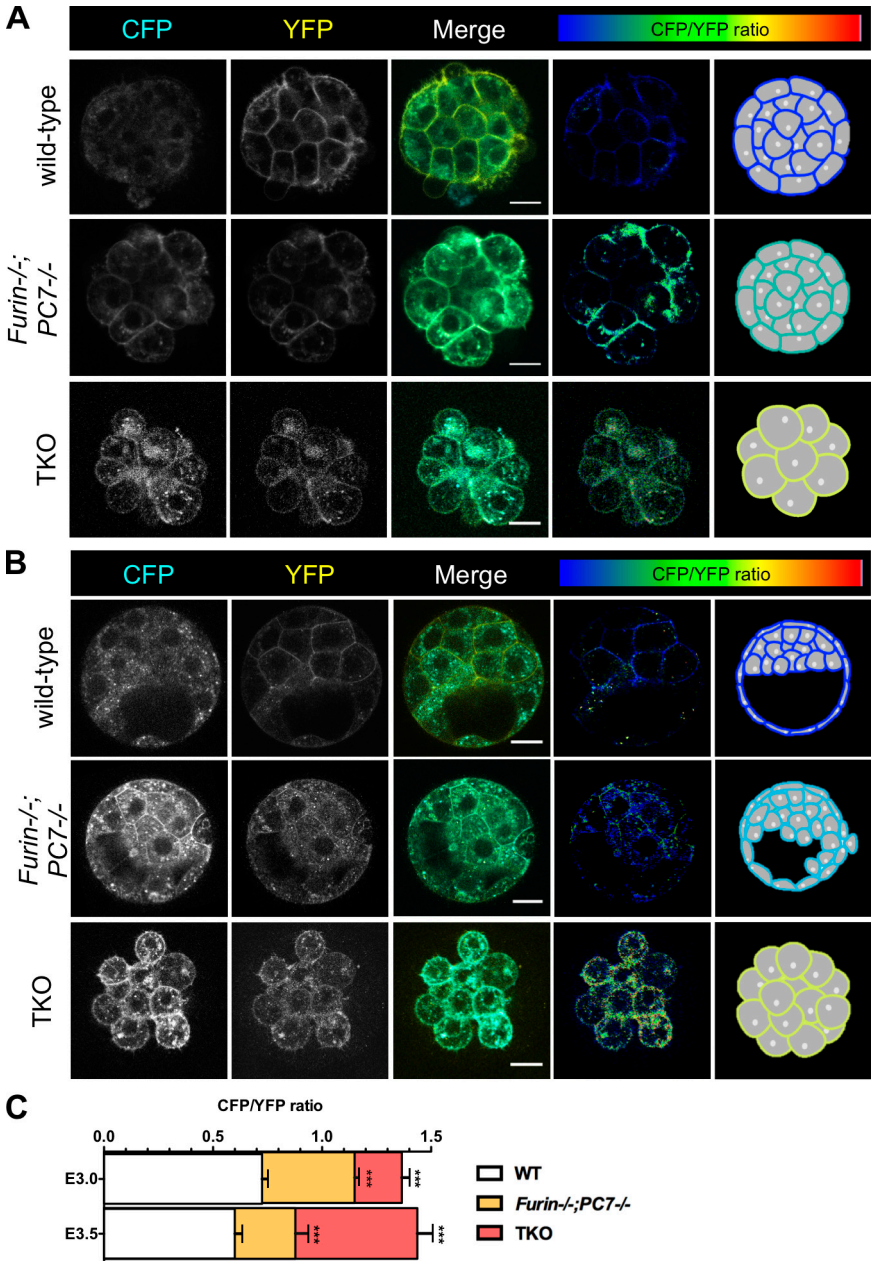

Figure 2. **Live imaging overlapping PC7, Furin, and Pace4 activities.** (A) Live CFP and YFP fluorescence of the transgenic reporter substrate CLIP in the wild-type (n = 6), *Furin*$^{-/-}$;*PC7*$^{-/-}$ (n = 5), and TKO mutants (n = 3) at E3.0. (B) Live CLIP imaging in wild-type (n = 6), *Furin*$^{-/-}$;*PC7*$^{-/-}$ (n = 5), and TKO embryos (n = 5) at E3.5. CFP/YFP heat maps of CLIP processing and their graphic summaries are shown in the last two columns. (C) Overlayed histograms of mean CFP/YFP ratios (n = 5 for each genotype; four independent experiments) at E3.0 versus E3.5. Values correspond to mean ± SEM. ***, P < 0.001; Student's t test. WT, wild type. Bars, 20 µm.

expressing the transgenic reporter substrate CLIP. Although lack of expression of the CLIP transgene before E2.5 precluded analysis at the earliest stages, CLIP imaging was possible starting at E3.0. Therefore, mutant embryos and control littermates carrying the CLIP transgene were cultured from E2.5 until the stages of interest, followed by ratiometric imaging of eCFP and citrine (YFP) fluorescence intensities. At the late morula stage (E3.0), all cells showed strong YFP signals at the plasma membrane, whereas eCFP fluorescence of CLIP was not above background either in wild-type embryos or in *Furin* or *PC7* single mutants (Fig. 2 A and Fig. S3 A), suggesting that CLIP was efficiently processed. In sharp contrast, *Furin;PC7* DKO embryos retained both YFP and CFP fluorescence at the plasma membrane. Quantification at E3.0 in randomly chosen inner and outer cells thus revealed a significantly elevated CFP/YFP ratio of 1.13 in DKO compared with 0.73 in wild-type embryos, confirming a net decrease in PC activity. Also at E3.5, DKO embryos showed elevated CFP/YFP ratios, although CLIP cleavage progressively increased at this and during later stages (Fig. 2, B and C; Fig. S3 B; and Table S2). To test whether processing is partially rescued by *Pace4*, we crossed the CLIP transgene into a TKO mutant background. TKO embryos retained significantly more CFP fluorescence in all cells than either wild-type or DKO embryos both at E3.0 and E3.5 (Fig. 2, A and B; and Table S2; n = 8/8), and even though they were not viable at E4.5, they did not decrease their CFP/YFP ratios until at least E3.5 (Fig. 2 C; P = 0.28). In good agreement, similarly elevated CFP/YFP ratios were observed until E4.5 in normal embryos expressing the cleavage mutant biosensor CLIPm (Fig. S3 C), supporting the idea that no other PCs are active at morula and blastocyst stages. Cleavage by maternal pools also seems improbable given that TKO embryos were unable to rescue CLIP processing or compaction at the morula stage. Thus, we conclude that a net increase in PC activity in DKO mutants is specifically mediated by Pace4 at E3.5.

Inhibition of CLIP processing reveals the lineage-specific distribution of Furin, PC7, and Pace4 activities at high spatial resolution

To assess the spatial distribution of individual PC activities, we compared CLIP processing in embryos cultured with or without the inhibitor deaconyl-Arg-Val-Lys-Arg-CMK. Concentrations of 5–75-µM CMK inhibit intracellular cleavage of the HIV gp160 precursor in Jurkat cells by 50–75% (Garten et al., 1994), and 10-µM CMK abolishes CLIP processing in HEK293T cells (Mesnard and Constam, 2010). Although a higher dose (20 µM) was toxic for uncompacted E2.5 wild-type embryos, incubation with 10-µM CMK within 30 h increased the CFP/YFP ratio of CLIP only 1.6-fold and only at the surface of ICM but not TE cells. However, significantly higher ratios were observed in DKO embryos even without CMK treatment (2.2- and 2.0-fold higher than the wild type in inner and outer cells, respectively; Fig. 3, A and B; and Table S3; $n = 8/8$ in each condition), suggesting that CMK efficacy was modest in the wild type and limited to inner cells. To address why CMK was so impotent especially in the TE lineage, we asked whether its efficacy can be unmasked in a PC mutant. Indeed, *PC7*$^{-/-}$ embryos that were treated with CMK accumulated more uncleaved CLIP than DKO mutants and often failed to cavitate ($n = 3/5$), indicating that CMK efficiently inhibited Furin activity in inner and outer cells (compare Fig. 3 [A and B] with Fig. 2 [B and C] and Table S3). In contrast, CMK-treated *Furin*$^{-/-}$ mutants cavitated and cleaved CLIP similar to the wild type, at least in TE. Compared with CMK-treated DKO embryos, they also more efficiently processed CLIP in the ICM. These results suggest that PC7 is relatively insensitive to CMK compared with Furin. Surprisingly, CMK treatment and loss of *Furin* nonetheless synergized to inhibit CLIP cleavage in the ICM (Fig. 3 B and Table S3). Moreover, a comparison with TKOs revealed that this synergism persisted in DKO mutants independently of *PC7*. Thus, we conclude that loss of *Furin* leads to compensatory up-regulation of CMK-sensitive Pace4 activity in the ICM. In sharp contrast, CFP/YFP ratios in the outer cells of CMK-treated DKOs remained 1.5-fold lower than those in TKOs, indicating that Pace4 activity in the TE lineage is CMK resistant. To investigate whether CMK sensitivity in inner cells might reflect a more accessible distribution of Pace4 in postsecretory compartments, we directly monitored the expression of PCs by quantitative RT-PCR (qRT-PCR) analysis in ICM and TE cells that were immunoisolated from blastocysts. Whereas *PC7* and *Furin* were ubiquitously expressed in both ICM and TE, *Pace4* was specifically transcribed in TE (Fig. S4). Therefore, the CMK-sensitive fraction of Pace4 in the ICM likely corresponds to secreted activity after its release by the TE. Whether an additional PC activity is present earlier remains unknown because 10-µM CMK as well as empty vehicle (DMSO) treatments led to premature developmental arrest of TKO embryos before the appearance of CLIP expression (unpublished data). Overall, our findings demonstrate that Furin, PC7, and Pace4 are all active in inner and outer cells but that they are differentially inhibited in these compartments by 10-µM CMK, with Furin being blocked in both TE and ICM lineages, PC7 in none, and Pace4 only in the ICM.

Furin and PC7 activities promote the segregation of TE and cooperate with Pace4 in ICM specification

Compaction and ICM formation depend on cell adhesion mediated by E-cadherin (Stephenson et al., 2012). Because compaction also required overlapping Furin, PC7, and Pace4 activities, we investigated whether E-cadherin–dependent fate decisions are impaired in DKO or TKO mutants. Triple labeling of late blastocysts (E4.0) with antibodies against the lineage markers Oct4 and Cdx2 and with the DNA stain Draq5 revealed similar proportions of ICM and TE cells in wild-type and DKO embryos (Fig. 4, A and B; and Table S4). Moreover, contrary to E-cadherin mutants (Stephenson et al., 2010), DKO embryos showed no ectopic Cdx2 staining in inner cells ($n = 7/7$). However, 10.0 ± 6.0% of their outer cells still coexpressed Cdx2 and Oct4, compared with only 0.6 ± 0.4% in the wild type, indicating that the TE is incorrectly specified. Interestingly, TKO embryos show a drastic increase of Cdx2-positive cells (Fig. 4, A and B; and Table S4), even though the total number of cells was indistinguishable from the wild type (Fig. 4 C). Furthermore, 49% of inner cells in TKO embryos ($n = 6/6$) showed ectopic Cdx2 staining at the expense of Oct4. In addition, similar to what we observed in DKO mutants, some Cdx2-positive cells in TKO embryos (7.0 ± 2.0%) failed to down-regulate Oct4 expression, confirming that PCs are required for the proper specification of TE cells. A net enrichment of TE relative to ICM cells also occurs in E-cadherin mutants, and this has been attributed to ectopic nuclear accumulation of YAP (Nishioka et al., 2009; Stephenson et al., 2010; Cockburn et al., 2013; Hirate et al., 2013). To evaluate whether this lineage decision requires functionally overlapping PC activities, we analyzed the distribution of YAP by immunostaining. Interestingly, TKO ectopically expressed nuclear YAP in almost all outer and inner cells (Fig. 4 D), indicating that ectopic outer cell fate correlates with ectopic nuclear YAP.

Role of PCs in E-cadherin precursor cleavage

Because TKO embryos lose E-cadherin expression at the plasma membrane and phenocopy E-cadherin mutants, we hypothesized that overlapping activities of PC7, Furin, and Pace4 may be responsible for E-cadherin precursor processing. To test this, we assessed whether E-cadherin precursor cleavage can be inhibited by PC-specific siRNAs or by CMK treatment in cultured cells. Concurring with earlier studies, HepG2, HEK293T, and LoVo cells all express *FURIN*, *PACE4*, *PC5/6*, and *PC7* mRNAs (Fig. 5 A; Hatsuzawa et al., 1990; Miranda et al., 1996; Seidah et al., 1996; Hallenberger et al., 1997). Furin is not functional, though, in LoVo cells (Takahashi et al., 1995). Western blot analysis of endogenous E-cadherin showed that whereas processing was diminished by up to 25% already at a low dose of 10-µM CMK, 40–80% remained uncleaved in all of the cell lines tested, even at a high dose of 100-µM CMK (Fig. 5 B). These data suggest that CMK only partially inhibits endogenous PC activity, or that various cell types activate E-cadherin partly by an unrelated protease. To distinguish between these possibilities, we chose HepG2 cells to test whether CMK treatment and depletion of *FURIN* or *PC7* have additive effects. We found that previously validated siRNAs deplete *FURIN* or *PC7* mRNAs or both by ∼60 and 40%, respectively, as described previously (Fig. S5; Scamuffa et al., 2008). Moreover, although knockdown of *FURIN* or *PC7* alone had little effect on E-cadherin, combined knockdown reduced processing by >40% (Fig. 5 C). Quantitative PCR revealed no compensatory up-regulation of *PACE4* mRNA expression (Fig. S3). Nevertheless, treatment

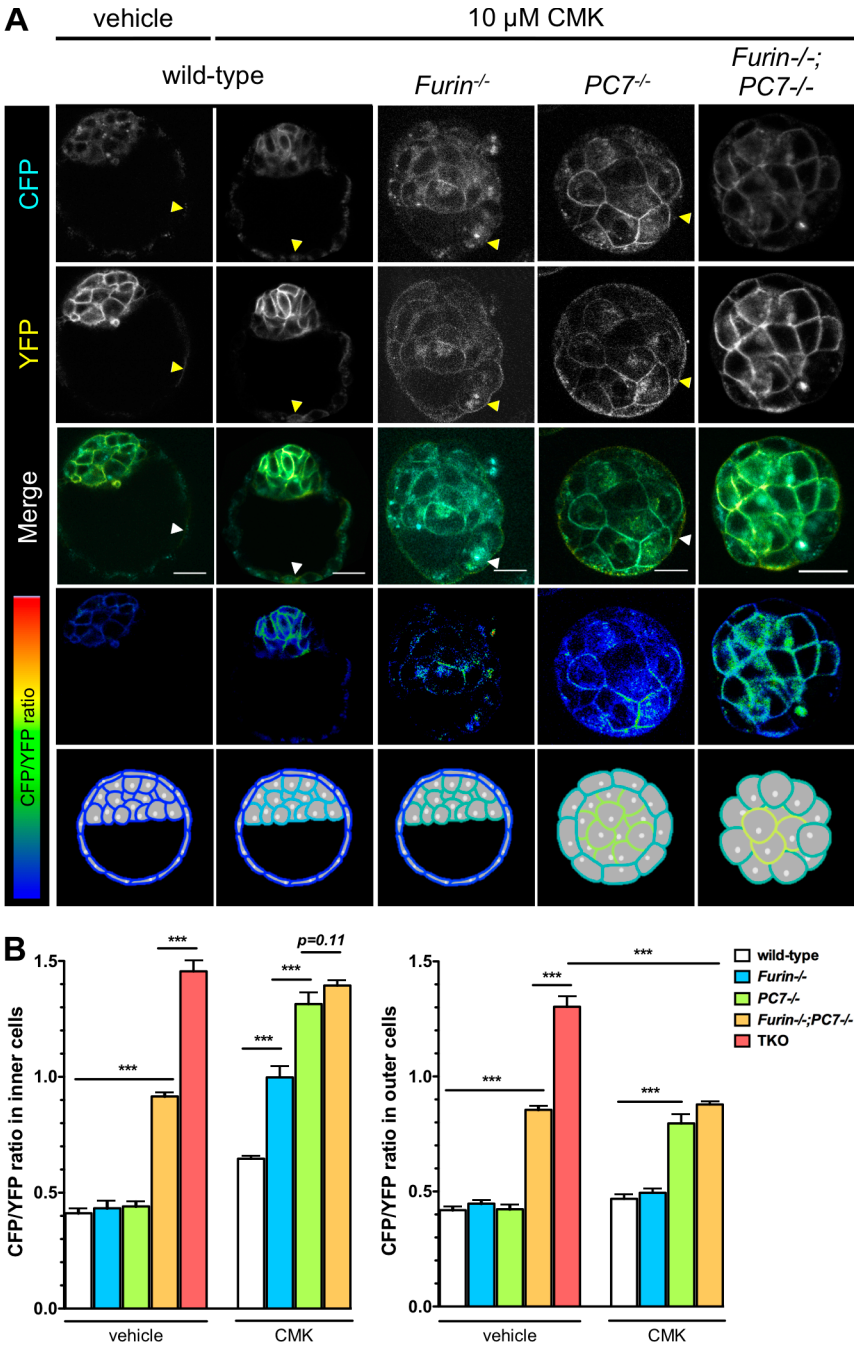

Figure 3. **Distribution and inhibitor profiles of Furin and PC7 activities.** (A) Distribution and mean CFP/YFP fluorescence ratios (heat maps) of CLIP in inner versus outer cells of live E3.5 wild-type embryos after culture in the absence (n = 8) or presence of 10-µM CMK (n = 8 wild-type; n = 6 *Furin*$^{-/-}$; n = 5 *PC7*$^{-/-}$; and n = 6 *Furin*$^{-/-}$;*PC7*$^{-/-}$ embryos) coupled with heat map and graphic summaries of CLIP processing. Arrowheads highlight lack of co-localization of CFP with YFP in outer cells. Bars, 20 µm. (B) Mean CFP/YFP ratios in inner (left) and outer cells (right) after treatment with empty vehicle or 10-µM CMK (n = 8 for the wild type and n = 5 for all other genotypes; TKO treated with CMK was not viable). Values correspond to mean ± SEM (*, P < 0.05; ***, P < 0.001; Student's t test).

of double knockdown cells with 10-µM CMK further reduced the residual processing to 10%. Also, when added with siPC7 alone, CMK reduced cleavage in an additive manner to <25%, whereas only a minimal additive effect of CMK was observed with *siFURIN* compared with CMK alone. These results confirm that Furin, but not PC7, is sensitive to inhibition by CMK in vivo. CMK treatment also inhibited cavitation and partially inhibited E-cadherin processing in *PC7*$^{-/-}$, but not in wild-type blastocysts (Figs. 5 D and 3 A). In addition, *PC7* RNAi synergized with the genetic ablation of *Furin* and *Pace4* to inhibit E-cadherin processing in mouse ES cells (Fig. 5, E and F). Overall, these results show that PC7 together with functionally overlapping activities mediates E-cadherin precursor cleavage both in vivo and in cultured mouse ES cells and transformed human cell lines.

Discussion

PCs can process multiple secreted proteins in cell-based assays, but in vivo functions are ill defined. Here, a targeted deletion of *PC7* unmasked functional overlap with *Furin* and *Pace4* in regulating cell polarization and adhesion during morula compaction and in localizing YAP signals that mediate the segregation of the ICM from the TE. Live imaging using the transgenic biosensor CLIP revealed that all of these PCs were active both in inner and outer cells and that partial rescue of *Furin;PC7* DKO embryos by *Pace4* temporally coincided with an up-regulation of Pace4 activity after E3.0. Consistent with their new role in ICM specification, Furin and PC7 each also promoted the processing and cell surface localization of E-cadherin. Our findings suggest that the mechanism to segregate the pluripo-

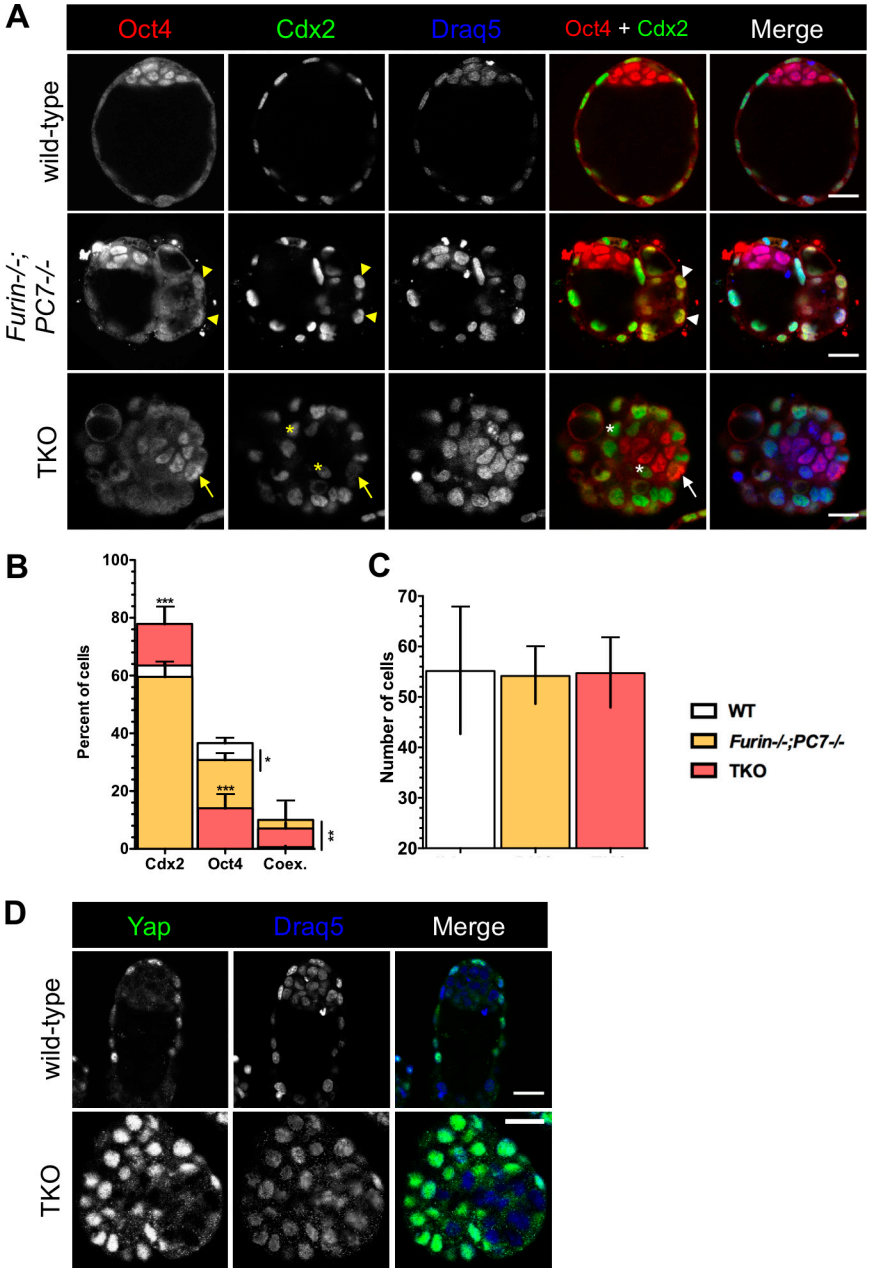

Figure 4. **Overlapping PC7, Furin, and Pace4 activities promote lineage segregation of inner and outer cells.** (A) Immunofluorescent staining of outer and inner cells by anti-Cdx2 (green) and anti-Oct4 antibodies (red) in E4.0 wild-type (n = 8), *Furin*$^{-/-}$;*PC7*$^{-/-}$ (n = 7), and TKO mutants (n = 6). Nuclei are marked by the DNA labeling reagent Draq5 (blue). Arrowheads point to outer cells stained for both Oct4 and Cdx2. The arrows indicate Oct4-positive outer cells lacking Cdx2, and asterisks indicate inner cells expressing ectopic Cdx2. (B) Overlayed histogram showing the percentage of cells that express Cdx2, Oct4, or both at E4.0 in wild-type, DKO, and TKO embryos. Values correspond to mean ± SEM. (C) Histogram showing the total number of cells in the wild type (WT; n = 8), *Furin*$^{-/-}$;*PC7*$^{-/-}$ (n = 7), and TKO (n = 6). Values correspond to mean ± SD. (D) Yap immunolocalization in the wild-type (n = 6) and TKO mutants (n = 3) at E4.0. *, P < 0.05; **, P < 0.01; ***, P < 0.001; Mann-Whitney test. Bars, 20 µm.

tent ICM from differentiating TE involves dynamic regulation of E-cadherin maturation by multiple PCs.

PC7$^{-/-}$;*Furin*$^{-/-}$;*Pace4*$^{-/-}$ TKO embryos showed impaired segregation of ICM from TE, marked by ectopic nuclear YAP and Cdx2 expression in half of all inner cells. Interestingly, these ectopic Cdx2-expressing cells continued to accumulate peripheral to the remaining Oct4-positive ICM, possibly reflecting differential adhesiveness. Their shapes were less hexagonal and more round than in the wild type, at least on the side facing the outermost TE layer, pointing to loosened contacts especially with outer neighbors. In keeping with impaired cell adhesion, TKO mutants also failed to compact at the morula stage. When detached from the TE by immunosurgery, the ICM spontaneously regenerates outer fates (Handyside, 1978; Hogan and Tilly, 1978; Spindle, 1978). Even in cells that normally do not reside at the surface, severing adhesion might prompt cell flattening and TE differentiation by alleviating cortical tension (Dard et al., 2009). In addition, diminished adhesion is expected to influence cell polarization because surfaces that cannot engage E-cadherin in contacts with neighboring cells accumulate aPKC (Stephenson et al., 2010). Activation of aPKC in turn blocks the kinases Lats1/2 to enable the assembly of nuclear complexes of YAP with Tead4 and thereby induces TE differentiation and *Cdx2* expression (Plusa et al., 2005; Yagi et al., 2007; Ralston and Rossant, 2008; Dard et al., 2009; Nishioka et al., 2009; Hirate et al., 2013). Thus, defective morula compaction, ectopic aPKC accumulation, and nuclear YAP and Cdx2 staining in inner cells of TKO mutants likely reflect impaired cell adhesion (Fig. 6).

The combination of impaired cell adhesion, delayed compaction, and disorganized apical-basal cell polarization seen in TKO mutants is reminiscent of embryos lacking E-cadherin. Adherens junctions are required for the assembly of tight junctions (Eckert and Fleming, 2008), and apical and basolateral

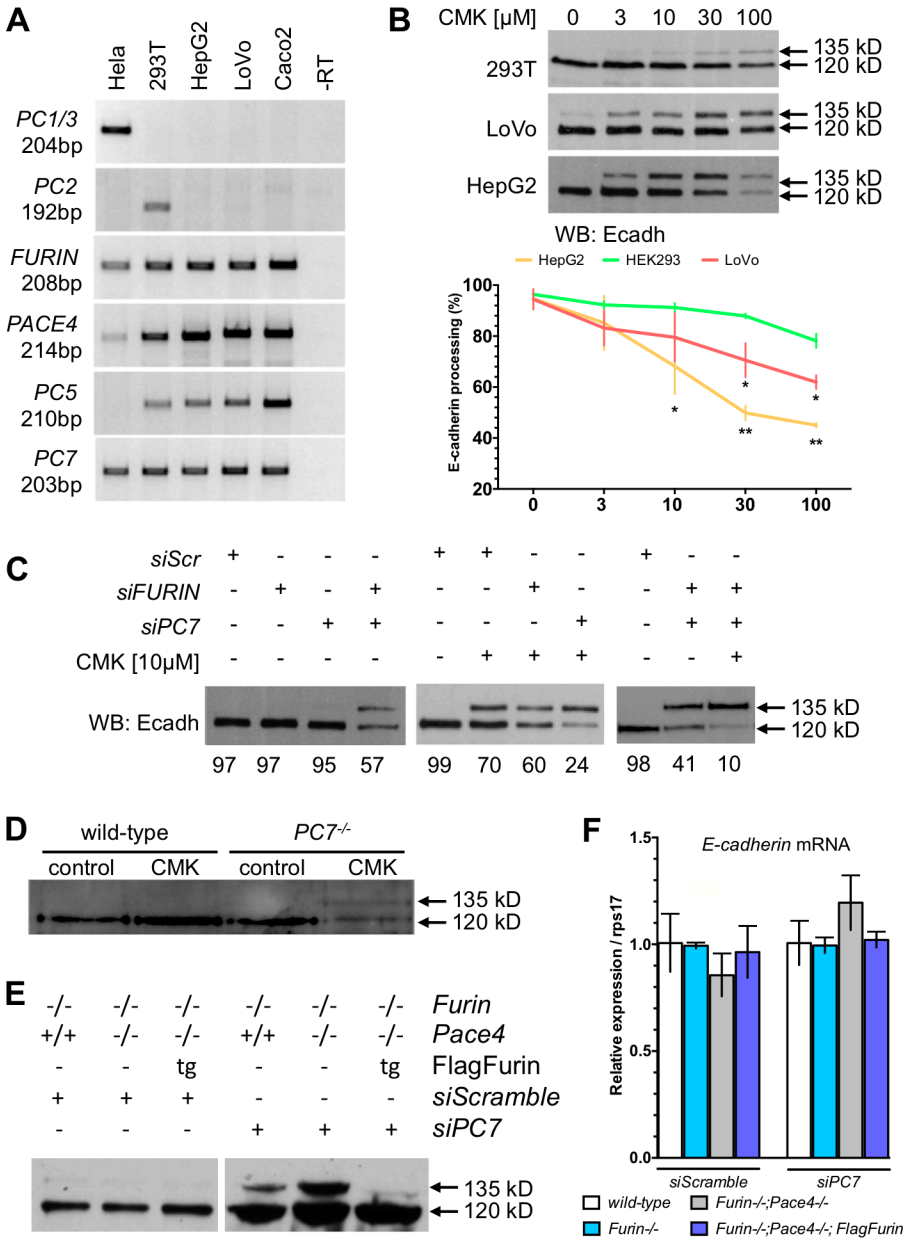

Figure 5. **Overlapping PC activities are required for E-cadherin precursor processing.** (A) Representative RT-PCR analysis of PC mRNAs in HeLa, 293T, HepG2, LoVo, and Caco2 cells (three independent experiments). (B, top) Representative Western blot (WB) analysis of E-cadherin processing in 293T, LoVo, and HepG2 cells that were treated with increasing concentrations of the pan-PC inhibitor decanoyl-RVKR-CMK (CMK). (Bottom) Compilation of four independent experiments. (C) Combination of CMK treatment and *FURIN* and *PC7* knockdown by specific siRNAs and their additive effects on the percentage (numbers at the bottom) of normal E-cadherin processing in HepG2 cells. Results are representative of three independent experiments. (D) Western blot analysis of E-cadherin in wild-type or *PC7*$^{-/-}$ embryos that were cultured in control condition or with 10-μM CMK from E2.5 to E3.5 (n = 33 embryos per genotype for each condition). The results shown were reproduced in two independent experiments. (E) Western blot analysis of E-cadherin in *Furin*$^{-/-}$, *Furin*$^{-/-}$;*Pace4*$^{-/-}$, or *Furin*$^{-/-}$;*Pace4*$^{-/-}$;*FurinTg* mouse ES cells that were transfected with 10-nM scrambled control or PC7 siRNAs. The results are representative of three independent experiments. (F) qRT-PCR analysis of the relative expression of E-cadherin in wild-type and mutant ES cells transfected with the indicated siRNAs (n = 3 experiments). *, $P < 0.05$; **, $P < 0.01$; Mann-Whitney test.

membrane domains fail to separate in the absence of E-cadherin (Stephenson et al., 2010). We found that although DKO embryos retained basolateral E-cadherin localization in at least some outer cells, assembly of tight junctions marked by ZO-1 staining and cavity formation were clearly perturbed. Furthermore, TKO embryos mislocalized E-cadherin to intracellular vesicles, and both outer and inner cells devoid of E-cadherin accumulated nonapical expression of aPKC. These observations agree with the notion that E-cadherin is essential to maintain epithelial cell polarity (Fig. 6 A; Stephenson et al., 2012). E-cadherin also mediates adhesion of filopodia and their myosin-induced traction on neighboring blastomeres of eight-cell stage embryos to initiate morula compaction (Fierro-González et al., 2013). Possibly, compaction of DKO embryos is delayed because of impaired adhesion of such filopodia.

Proteolytic maturation enables the extracellular domain of E-cadherin to engage in homotypic interactions (Ozawa and Kemler, 1990). Here, we found that combined depletion

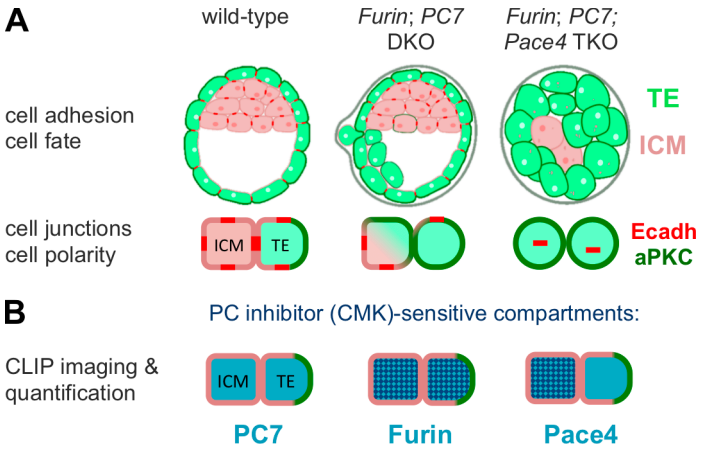

Figure 6. **Functionally overlapping activities of PC7, Furin, and Pace4 stimulate the polarization of outer cells and the specification of inner cells by E-cadherin.** (A) Schematic representation of *Furin*$^{-/-}$;*PC7*$^{-/-}$ and TKO mutant blastocysts. After a delay of compaction, cell adhesion mediated by E-cadherin can be significantly rescued in most blastomeres in *Furin*$^{-/-}$;*PC7*$^{-/-}$ mutants. In contrast, in triple mutants lacking Furin, PC7, and Pace4, E-cadherin is retained in the cytoplasm, leading to widely impaired cell adhesion and ectopic aPKC accumulation. (B) Map of PC activities and their differential sensitivity to the soluble inhibitor CMK obtained by CLIP imaging.

of *FURIN* and *PC7* by RNAi in human HepG2 hepatoma cells reduced E-cadherin processing by almost 60% and that the remaining activity dropped to 10% upon addition of the PC inhibitor CMK. E-cadherin cleavage also decreased in CMK-treated cells transfected with *PC7* siRNA alone, whereas *FURIN* siRNA alone failed to synergize with CMK. A role of endogenous Furin in E-cadherin precursor processing thus is masked in part by a CMK-resistant pool of PC7. Our discovery that PC7 and Furin respond differently to CMK provides an important simple criterion to assess their relative contributions to the processing of shared substrates. We also transfected siRNAs against *PACE4* or *PCSK5*, but these knockdowns were inefficient, precluding quantification of a potential synergism (unpublished data). As these PCs are present, one or both may contribute at least to the CMK-sensitive pool of E-cadherin processing activity in HepG2 cells. CMK treatment also reduced precursor processing in *PC7*$^{-/-}$ embryos and further delayed compaction of *Furin*$^{-/-}$;*PC7*$^{-/-}$ DKO mutants, even though it failed to do so in wild-type or *Furin*$^{-/-}$ morulae. Thus, Furin and CMK-resistant PC7 activities acting together with at least one partially CMK-sensitive convertase process E-cadherin both in vitro and in vivo. In good agreement, inactivation of three PCs was necessary to abolish E-cadherin cell surface localization in vivo. Because proteolytic maturation is essential for E-cadherin cell surface localization (Geng et al., 2012), it is plausible that PC7, Furin, and Pace4 enable TE cell polarization and ICM specification by jointly regulating E-cadherin cleavage.

We also mapped the distribution of PC activities and their sensitivity to CMK in vivo by CLIP imaging. Cleavage of CLIP in mouse blastocysts is enhanced by redundant Furin and Pace4 activities, but the time of onset of cleavage and a potential role of PC7 had not been analyzed (Mesnard and Constam, 2010; Mesnard et al., 2011). We found that the compaction and cavitation defects of *Furin*$^{-/-}$;*PC7*$^{-/-}$ mutants correlated with a severe inhibition of CLIP cleavage at the morula stage and that partial rescue of these processes coincided with a marked up-regulation of CLIP processing by Pace4 activity at E3.5. Moreover, CFP/YFP fluorescence ratios reached 1.6-fold higher values in inner than in outer cells only in DKO but not in wild-type embryos, and this difference was lost in TKO mutants, indicating that Pace4 was most active in outer cells. In keeping with this conclusion, zygotic *Pace4* expression has only been observed in the TE lineage and is stimulated by the TE-specific transcription factor Elf5 (Donnison et al., 2005; Mesnard et al., 2006). Accordingly, Pace4 activity in the ICM may be cell nonautonomous (Mesnard et al., 2011). In keeping with this interpretation, only the ICM-associated pool of Pace4 activity was inhibited by CMK. In sharp contrast, Furin and PC7 were blocked by CMK either in all cells or in none, respectively (Fig. 6 B). Importantly, CMK inhibits all of these PCs in cell-free assays, with K_i values of 0.1, 2.0, and 3.6 nM for PC7, Furin, and Pace4, respectively (Jean et al., 1998). CMK treatment also blocks extracellular Pace4 and sheds Furin activities in conditioned medium of ES cells (Mesnard and Constam, 2010). Together, these observations suggest that CMK-resistant PC activities reside in intracellular compartments that are less accessible than the CMK-sensitive pools of Furin and Pace4. In transfected cells, intracellular PC7 can rapidly enter post-Golgi compartments without passing through the trans-Golgi network (Rousselet et al., 2011). However, the trafficking itineraries of endogenous PC7 or Pace4 are unknown because of the lack of suitable antibodies. Our live imaging suggests that the abodes of these and other PC activities may be determined in future studies using compartment-specific CLIP variants to elucidate exactly where specific substrates are processed.

Does the enrichment of Pace4 activity in outer cells differentially modulate adhesive properties of E-cadherin compared with inner cells? Cells that lost contact with their neighbors in *Furin*$^{-/-}$;*PC7*$^{-/-}$ DKO embryos were always positioned at the periphery. These could be inner cells that normally do not express Pace4 and therefore failed to maintain their adherens junctions with ICM neighbors (Fig. 6 A). However,unlike TKO or CMK-treated DKO mutants, DKO mutants cultured without CMK largely maintained Oct4 expression and diminished the cleavage of CLIP in inner cells by only 50% compared to the wild type, suggesting that their CMK-sensitive pool of Pace4 activity substantially rescued adhesion even within the ICM. In contrast, in outer cells, Pace4 alone may fail to reliably maintain contacts because of their epithelialization. Polarized epithelial cells secrete Pace4 basolaterally, whereas a shed form of Furin is released on the apical side (Mesnard et al., 2011), indicating that progressive cell polarization and its maintenance by E-cadherin may eventually segregate these PCs into distinct compartments and thereby limit their functional redundancy. Moreover, because delivery of E-cadherin to adherens junctions in polarized cells involves Rab11 recycling endosomes (Golachowska et al., 2010), alternative PCs may ensure efficient cleavage along this unique transport route. Recent studies revealed that only outer cells also activate Notch-1, an unrelated PC substrate acting in parallel to Tead4 to reinforce *Cdx2* expression (Logeat et al., 1998; Rayon et al., 2014). However, if cell adhesion or Notch-1 processing are differentially regulated

in outer compared with inner cells because of Pace4, redundant mechanisms must exist that maintain both cell fates in *Pace4*$^{-/-}$ and other PC single mutants.

The spatiotemporal regulation of PC activities revealed by quantification of CLIP imaging at the morula stage suggests a role in modulating dynamic changes in cell adhesiveness and in the specification or maintenance of distinct cell fates. Interestingly, down-regulation of Furin and concomitant up-regulation of a secreted soluble isoform of PC5 in cancer cell lines from diverse tissues favor alternative cleavage of the related N-cadherin at a more distal site in the extracellular domain, thereby inhibiting instead of activating adhesive properties (Maret et al., 2012). It will therefore be important to investigate how dynamic changes in activity levels or subcellular localization of PCs influence epithelial–mesenchymal transitions and their reversion during cancer metastasis. Our finding that multiple overlapping PC activities can moonlight for one another to process E-cadherin suggests that future therapies targeting oncogenic PC activities individually should spare the function of this essential tumor suppressor.

Materials and methods

Derivation of PC7$^{-/-}$ mice

A *PC7* gene-targeting vector was derived from a 129 SvJ genomic phage library by flanking an inverted MC1-neomycin resistance cassette with 5′ and 3′ homology arms comprising a 4-kb NdeI–SalI and a 3.6-kb XbaI fragment of the *Pcsk7* locus. The linearized vector was electroporated into 129 Sv/Ev CCE ES cells. Deletion of a 6.2-kb SalI–XbaI fragment encoding the translational start site, the pro region, and the entire catalytic domain of PC7 by homologous recombination gave rise to the allele *Pcsk7*^{tm1Rob}. When injected into C57BL/6 blastocysts, two targeted ES clones gave rise to male germline chimeras that were backcrossed to C57BL/6 females. Intercrosses between heterozygous F1 progeny yielded fertile adult homozygotes without any overt abnormalities at a Mendelian frequency. To detect homologous recombination, genomic DNA samples were digested with XbaI and analyzed by Southern hybridization. A 0.9-kb KpnI–XbaI probe upstream of the integration site detected a 12-kb fragment in the wild type and a mutant 5.7-kb fragment. Homologous recombination was verified using a 0.5-kb XbaI fragment 3′ of the integration site, which detected 12-kb or 6.2-kb KpnI fragments corresponding to the wild-type or mutant alleles, respectively (Fig. S1 A). PCR genotyping was performed using the reverse primer 5′-AGCCATCATAGTTGCAGTTGTCATTGTG-3′ in conjunction with the forward primer 5′-CCTCTTCCCATCCCGCCTTCATTA-3′ and the neomycin-specific primer 5′-GGCTGCAGGGTCGCTCGGT-3′ at an annealing temperature of 59°C to simultaneously amplify a 652-bp and a 478-bp fragment of the wild-type and mutant alleles, respectively. Animals were maintained in individually ventilated cages at the specific pathogen-free animal facility of Ecole Polytechnique Fédérale de Lausanne (EPFL). Experiments were performed in accordance with Swiss guidelines for the care and use of laboratory animals.

Breeding and genotyping of compound mutant mice and embryos

PC7$^{+/-}$ heterozygous males on a mixed C57BL/6 × 129 SvEv background were backcrossed for >10 generations to C57BL/6 females. *PC7*$^{+/-}$ animals were backcrossed for at least four generations to *Furin*^{tm1Ajmr} (Roebroek et al., 1998) and *Pcsk6*^{tm1Rob} heterozygotes (Constam and Robertson, 2000) on an outbred NMRI background with the CLIP transgene (Mesnard and Constam, 2010). *Furin*^{tm1Ajmr} contains a 3-phosphoglycerate kinase promoter–hygromycin phosphotransferase and a stop codon that disrupts the *Furin* coding sequence in exon 4. In the *Pcsk6*^{tm1Rob} allele, an MCl-neomycin phosphotransferase cassette was inserted by homologous recombination to delete the coding region for the catalytic domain of Pace4. Compound mutants were intercrossed to obtain double or triple homozygous mutant embryos. PCR primers used for genotyping are described in Table S5, Table S6, and Table S7.

Cell transfection and culture of preimplantation embryos

The indicated human cell lines were cultured in DMEM containing 10% FBS and 1% penicillin/streptomycin (Gibco). Wild-type and mutant mouse ES cells were derived from blastocyst outgrowths in DMEM medium, 10% FBS, 5% knockout serum replacement (Invitrogen), and 30% ES cell–conditioned medium (Beck et al., 2002) and maintained on neomycin- and hygromycin-resistant STO fibroblasts in DMEM containing 15% FBS, β-mercaptoethanol, and 10^3 units of leukemia inhibitory factor. For stable transfection, mutant ES cells were electroporated with the mouse Furin coding sequence containing a FLAG epitope after the autocatalytic cleavage site and an EF1-α promoter followed by an IRESpac cassette for puromycin selection (Beck et al., 2002). Specific siRNAs against PCs (Scamuffa et al., 2008) were purchased from Ambion and transfected using Lipofectamine 2000 (Invitrogen). ES cells were transfected using Lipofectamine 2000 in feeder-free conditions. Embryos were flushed at E2.5–2.75 in PBS supplemented with 10% FBS, washed twice in equilibrated potassium-supplemented simplex optimized medium (KSOM; EMD Millipore), and cultured with intact zona pellucida in KSOM at 37°C and 5% CO_2 until the stage of interest. Where indicated, decanoyl-RVKR-CMK (Tocris Bioscience) or empty vehicle (DMSO) was added at the indicated concentrations and replaced every 12 h. All experiments were repeated on more than three littermates.

Estimation of biosensor cleavage

Live embryos were scanned in a 37°C/5% CO_2 chamber in individual microdrops of KSOM on glass-bottomed microwell dishes (MatTek Corporation) at high speed (700 Hz) on a confocal microscope (SP2 or SP5; Leica) with Leica software (LAS AF 2009). All embryos were scanned using the same objective (HC Plan Apochromat 20×/0.70 NA; immersion), with a pinhole of 1 airy unit, a voxel size of 75 nm, 25% laser intensity, and number of z section. The gain of the photomultiplier was constant at any given stage but adapted to increasing CLIP expression levels at late compared with early stages. Heat maps were imaged using a fluorescence resonance energy transfer Ratio-Quantification plugin developed by the EPFL bioimaging platform. The YFP channel served as the reference channel and to define signal thresholds. Corresponding images of fluorescence ratios were colored using the Rainbow RGB.lut and a median filter of 1.0 pixel. For CFP/YFP ratio quantification, 7–15 random membrane regions were selected per embryo and quantified using Fiji. Each region of interest (ROI) was drawn on a magnified YFP channel and applied on a CFP channel. The mean of YFP and CFP background fluorescence was measured on 50 ROIs from 10 nontransgenic embryos scanned with the same conditions as mentioned before. After subtraction of this background, CFP and YFP signals of CLIP in individual ROIs were each divided by the gain of photomultiplier for signal normalization. The resulting corrected CFP values were then divided by their corresponding corrected YFP values in every ROI to obtain individual CFP/YFP ratios. Mean CFP/YFP ratios of up to 100 ROIs are displayed in arbitrary units (Table S2). For quantification of inner versus outer cells, ROIs in outer cells were drawn at cell–cell contacts between two outer cells and at membranes at the embryo surface, whereas ROIs in inner cells were drawn at cell–cell contacts between two inner cells. Cell–cell contacts between outer and inner cells were

not considered in these experiments. All experiments were repeated on more than three littermates.

Indirect immunofluorescent stainings

Embryos were fixed in 4% PFA, washed three times in PBS containing 0.1% Triton X-100, and incubated in 10% FBS for 1 h. Primary antibodies were incubated overnight at 4°C. Antibodies included anti-Oct4 (sc-8628; Santa Cruz Biotechnology, Inc.), anti-Cdx2 (MU392A-UC; Biogenex), anti-Yap (4912S; Cell Signaling Technology), anti-aPKC (sc-216; Santa Cruz Biotechnology, Inc.), anti–E-cadherin (U3254; Sigma-Aldrich), and anti–ZO-1 (sc-10804; Santa Cruz Biotechnology, Inc.). Embryos were washed three times in PBS/0.1% Triton X-100, and secondary antibodies coupled with Alexa Fluor 488, 568, and 647 (Jackson ImmunoResearch Laboratories, Inc.) and Draq5 were incubated at room temperature for 2 h, washed three times with PBS/0.1% Triton X-100, and analyzed at room temperature in individual microdrops of PBS/0.1% Triton X-100 on glass-bottomed microwell dishes at room temperature (19–21°C) using the confocal microscopy procedure as described in the previous section (Bessonnard et al., 2014). Images were prepared using Fiji and Gimp 2.8 software. Quantification of fluorescence was done as previously described for CFP/YFP ratiometric analyses. All experiments were repeated on more than three littermates.

Gene expression analysis

Total mRNA was isolated using TRIzol, reverse transcribed using Superscript III (Invitrogen), and analyzed using SYBR green PCR Master Mix (Applied Biosystems) coupled with 7900ht Fast RT-PCR system (Applied Biosystems). Human qRT-PCR primers were designed using Primer Blast (National Center for Biotechnology Information) and are described in Table S6. Proteins were extracted in PBS supplemented with 1% (vol/vol) Triton X-100, 1-mM EDTA, and protease inhibitor cocktail (Roche). E-cadherin protein was analyzed by Western blotting using rat anti–E-cadherin antibody (U3254; Sigma-Aldrich), anti–rat IgG-HRP secondary antibody (Jackson ImmunoResearch Laboratories, Inc.), and Western Lightning ECL kit (Thermo Fisher Scientific). E3.5 wild-type embryos were flushed in M2 medium (Sigma-Aldrich). Zona pellucida was removed with Tyrode's acid (Sigma-Aldrich) and incubated for 10 min with anti–mouse antibody (Sigma-Aldrich) at 37°C and with guinea pig complement serum at 37°C for 30 min (Sigma-Aldrich). Three embryos or six resulting TE/ICMs were pooled together, and mRNA was isolated using TRIzol (Nishioka et al., 2009), reverse transcribed using Superscript VILO (Invitrogen), and analyzed using SYBR green PCR Master Mix. Mouse qRT-PCR primers (Table S7) were designed using Primer Blast.

Statistical analysis

Statistical tests were performed as described using Prism (GraphPad Software). The normal distribution of CFP/YFP ratio values and ICM/TE distribution were verified with the Shapiro-Wilk normality test, and results were analyzed by a Mann-Whitney or by a Student's *t* test depending on previous results. Mendelian distribution was analyzed using a χ^2 test.

Online supplemental material

Fig. S1 shows the knockout strategy in the PC7 locus. Fig. S2 shows E-cadherin/aPKC expression profiles in cultured or fresh embryos. Fig. S3 shows CFP/YFP ratios of CLIPv0 and CLIPm transgenes in several mutant embryos. Fig. S4 represents results obtained with embryo immunosurgery combined with qRT-PCR. Fig. S5 shows knockdown efficiencies in HepG2 cells. Table S1 recapitulates the cavity formation during development in wild-type, DKO, and TKO embryos. Table S2 summarizes CFP/YFP ratios at E3.0, E3.5, and E4.5. Table S3 summarizes CFP/YFP ratios in ICM or TE cells in control conditions or after CMK treatment (10 µM). Table S4 recapitulates the percentage of ICM/TE cells observed at E4.0 in wild-type, DKO, and TKO embryos. Tables S5, S6, and S7 correspond to the list of primers used for genotyping and gene expression profiling. Online supplemental material is available at http://www.jcb.org/cgi/content/full/jcb.201503042/DC1. Additional data are available in the JCB DataViewer at http://dx.doi.org/10.1083/jcb.201503042.dv.

Acknowledgments

We would like to thank the animal core facility of the EPFL School of Life Sciences for help with the maintenance of transgenic mice. We also thank the EPFL bioimaging core facility for advice on image acquisition and analysis, Dr. Michel Cohen-Tannoudji and Sandrine Vandormael-Pournin (Paris) for advice on ES cell manipulations, and Dr. Claire Chazaud (Clermont-Ferrand) and members of the Constam laboratory for comments on this manuscript.

This project was supported by the Swiss National Science Foundation (grant 3100A0-118080/1) and by EU FP6 MEMORIES Project (grant no. 037831) to D.B. Constam.

The authors declare no competing financial interests.

Author contributions: D. Mesnard and D.B. Constam conceived and designed initial experiments. D. Mesnard performed experiments on DKO embryos and human-derived cells and initiated biosensor analysis. S. Bessonnard performed experiments on TKO embryos, ES cells, immunosurgery, and fluorescent quantification. S. Bessonnard, D. Mesnard, and D.B. Constam analyzed the data and wrote the manuscript.

Submitted: 10 March 2015
Accepted: 5 August 2015

References

Anani, S., S. Bhat, N. Honma-Yamanaka, D. Krawchuk, and Y. Yamanaka. 2014. Initiation of Hippo signaling is linked to polarity rather than to cell position in the pre-implantation mouse embryo. *Development.* 141:2813–2824. http://dx.doi.org/10.1242/dev.107276

Beck, S., J.A. Le Good, M. Guzman, N. Ben Haim, K. Roy, F. Beermann, and D.B. Constam. 2002. Extraembryonic proteases regulate Nodal signalling during gastrulation. *Nat. Cell Biol.* 4:981–985. http://dx.doi.org/10.1038/ncb890

Bessonnard, S., L. De Mot, D. Gonze, M. Barriol, C. Dennis, A. Goldbeter, G. Dupont, and C. Chazaud. 2014. Gata6, Nanog and Erk signaling control cell fate in the inner cell mass through a tristable regulatory network. *Development.* 141:3637–3648. http://dx.doi.org/10.1242/dev.109678

Bischoff, M., D.E. Parfitt, and M. Zernicka-Goetz. 2008. Formation of the embryonic-abembryonic axis of the mouse blastocyst: Relationships between orientation of early cleavage divisions and pattern of symmetric/asymmetric divisions. *Development.* 135:953–962. http://dx.doi.org/10.1242/dev.014316

Bosshart, H., J. Humphrey, E. Deignan, J. Davidson, J. Drazba, L. Yuan, V. Oorschot, P.J. Peters, and J.S. Bonifacino. 1994. The cytoplasmic domain mediates localization of furin to the trans-Golgi network en route to the endosomal/lysosomal system. *J. Cell Biol.* 126:1157–1172. http://dx.doi.org/10.1083/jcb.126.5.1157

Brasch, J., O.J. Harrison, B. Honig, and L. Shapiro. 2012. Thinking outside the cell: How cadherins drive adhesion. *Trends Cell Biol.* 22:299–310. http://dx.doi.org/10.1016/j.tcb.2012.03.004

Burton, A., J. Muller, S. Tu, P. Padilla-Longoria, E. Guccione, and M.E. Torres-Padilla. 2013. Single-cell profiling of epigenetic modifiers identifies PRDM14 as an inducer of cell fate in the mammalian embryo. *Cell Reports.* 5:687–701. http://dx.doi.org/10.1016/j.celrep.2013.09.044

Cockburn, K., S. Biechele, J. Garner, and J. Rossant. 2013. The Hippo pathway member Nf2 is required for inner cell mass specification. *Curr. Biol.* 23:1195–1201. http://dx.doi.org/10.1016/j.cub.2013.05.044

Constam, D.B., and E.J. Robertson. 2000. SPC4/PACE4 regulates a TGFβ signaling network during axis formation. *Genes Dev.* 14:1146–1155.

Dard, N., T. Le, B. Maro, and S. Louvet-Vallée. 2009. Inactivation of aPKCλ reveals a context dependent allocation of cell lineages in preimplantation mouse embryos. *PLoS ONE.* 4:e7117. http://dx.doi.org/10.1371/journal.pone.0007117

Denault, J., L. Bissonnette, J. Longpré, G. Charest, P. Lavigne, and R. Leduc. 2002. Ectodomain shedding of furin: Kinetics and role of the cysteine-rich region. *FEBS Lett.* 527:309–314. http://dx.doi.org/10.1016/S0014-5793(02)03249-0

Dietrich, J.E., and T. Hiiragi. 2007. Stochastic patterning in the mouse pre-implantation embryo. *Development.* 134:4219–4231. http://dx.doi.org/10.1242/dev.003798

Donnison, M., A. Beaton, H.W. Davey, R. Broadhurst, P. L'Huillier, and P.L. Pfeffer. 2005. Loss of the extraembryonic ectoderm in Elf5 mutants leads to defects in embryonic patterning. *Development.* 132:2299–2308. http://dx.doi.org/10.1242/dev.01819

Eckert, J.J., and T.P. Fleming. 2008. Tight junction biogenesis during early development. *Biochim. Biophys. Acta.* 1778:717–728. http://dx.doi.org/10.1016/j.bbamem.2007.09.031

Eckert, J.J., A. McCallum, A. Mears, M.G. Rumsby, I.T. Cameron, and T.P. Fleming. 2004. Specific PKC isoforms regulate blastocoel formation during mouse preimplantation development. *Dev. Biol.* 274:384–401. http://dx.doi.org/10.1016/j.ydbio.2004.07.027

Eckert, J.J., A. McCallum, A. Mears, M.G. Rumsby, I.T. Cameron, and T.P. Fleming. 2005. Relative contribution of cell contact pattern, specific PKC isoforms and gap junctional communication in tight junction assembly in the mouse early embryo. *Dev. Biol.* 288:234–247. http://dx.doi.org/10.1016/j.ydbio.2005.09.037

Fierro-González, J.C., M.D. White, J.C. Silva, and N. Plachta. 2013. Cadherin-dependent filopodia control preimplantation embryo compaction. *Nat. Cell Biol.* 15:1424–1433. http://dx.doi.org/10.1038/ncb2875

Fleming, T.P. 1987. A quantitative analysis of cell allocation to trophectoderm and inner cell mass in the mouse blastocyst. *Dev. Biol.* 119:520–531. http://dx.doi.org/10.1016/0012-1606(87)90055-8

Garten, W., S. Hallenberger, D. Ortmann, W. Schäfer, M. Vey, H. Angliker, E. Shaw, and H.D. Klenk. 1994. Processing of viral glycoproteins by the subtilisin-like endoprotease furin and its inhibition by specific peptidylchloroalkylketones. *Biochimie.* 76:217–225. http://dx.doi.org/10.1016/0300-9084(94)90149-X

Geng, F., W. Zhu, R.A. Anderson, B. Leber, and D.W. Andrews. 2012. Multiple post-translational modifications regulate E-cadherin transport during apoptosis. *J. Cell Sci.* 125:2615–2625. http://dx.doi.org/10.1242/jcs.096735

Golachowska, M.R., D. Hoekstra, and S.C. van IJzendoorn. 2010. Recycling endosomes in apical plasma membrane domain formation and epithelial cell polarity. *Trends Cell Biol.* 20:618–626. http://dx.doi.org/10.1016/j.tcb.2010.08.004

Hallenberger, S., M. Moulard, M. Sordel, H.D. Klenk, and W. Garten. 1997. The role of eukaryotic subtilisin-like endoproteases for the activation of human immunodeficiency virus glycoproteins in natural host cells. *J. Virol.* 71:1036–1045.

Handyside, A.H. 1978. Time of commitment of inside cells isolated from preimplantation mouse embryos. *J. Embryol. Exp. Morphol.* 45:37–53.

Handyside, A.H. 1980. Distribution of antibody- and lectin-binding sites on dissociated blastomeres from mouse morulae: Evidence for polarization at compaction. *J. Embryol. Exp. Morphol.* 60:99–116.

Hatsuzawa, K., M. Hosaka, T. Nakagawa, M. Nagase, A. Shoda, K. Murakami, and K. Nakayama. 1990. Structure and expression of mouse furin, a yeast Kex2-related protease. Lack of processing of coexpressed prorenin in GH4C1 cells. *J. Biol. Chem.* 265:22075–22078.

Hillman, N., M.I. Sherman, and C. Graham. 1972. The effect of spatial arrangement on cell determination during mouse development. *J. Embryol. Exp. Morphol.* 28:263–278.

Hirate, Y., S. Hirahara, K. Inoue, A. Suzuki, V.B. Alarcon, K. Akimoto, T. Hirai, T. Hara, M. Adachi, K. Chida, et al. 2013. Polarity-dependent distribution of angiomotin localizes Hippo signaling in preimplantation embryos. *Curr. Biol.* 23:1181–1194. http://dx.doi.org/10.1016/j.cub.2013.05.014

Hogan, B., and R. Tilly. 1978. In vitro development of inner cell masses isolated immunosurgically from mouse blastocysts. II. Inner cell masses from 3.5- to 4.0-day p.c. blastocysts. *J. Embryol. Exp. Morphol.* 45:107–121.

Jean, F., K. Stella, L. Thomas, G. Liu, Y. Xiang, A.J. Reason, and G. Thomas. 1998. α_1-Antitrypsin Portland, a bioengineered serpin highly selective for furin: Application as an antipathogenic agent. *Proc. Natl. Acad. Sci. USA.* 95:7293–7298. http://dx.doi.org/10.1073/pnas.95.13.7293

Johnson, M.H., and C.A. Ziomek. 1981. The foundation of two distinct cell lineages within the mouse morula. *Cell.* 24:71–80. http://dx.doi.org/10.1016/0092-8674(81)90502-X

Johnson, M.H., and C.A. Ziomek. 1983. Cell interactions influence the fate of mouse blastomeres undergoing the transition from the 16- to the 32-cell stage. *Dev. Biol.* 95:211–218. http://dx.doi.org/10.1016/0012-1606(83)90019-2

Leung, C.Y., and M. Zernicka-Goetz. 2013. Angiomotin prevents pluripotent lineage differentiation in mouse embryos via Hippo pathway-dependent and -independent mechanisms. *Nat. Commun.* 4:2251. http://dx.doi.org/10.1038/ncomms3251

Logeat, F., C. Bessia, C. Brou, O. LeBail, S. Jarriault, N.G. Seidah, and A. Israël. 1998. The Notch1 receptor is cleaved constitutively by a furin-like convertase. *Proc. Natl. Acad. Sci. USA.* 95:8108–8112. http://dx.doi.org/10.1073/pnas.95.14.8108

Maret, D., M.S. Sadr, E.S. Sadr, D.R. Colman, R.F. Del Maestro, and N.G. Seidah. 2012. Opposite roles of furin and PC5A in N-cadherin processing. *Neoplasia.* 14:880–892. http://dx.doi.org/10.1593/neo.121250

McDole, K., Y. Xiong, P.A. Iglesias, and Y. Zheng. 2011. Lineage mapping the pre-implantation mouse embryo by two-photon microscopy, new insights into the segregation of cell fates. *Dev. Biol.* 355:239–249. http://dx.doi.org/10.1016/j.ydbio.2011.04.024

Mesnard, D., and D.B. Constam. 2010. Imaging proprotein convertase activities and their regulation in the implanting mouse blastocyst. *J. Cell Biol.* 191:129–139. http://dx.doi.org/10.1083/jcb.201005026

Mesnard, D., M. Guzman-Ayala, and D.B. Constam. 2006. Nodal specifies embryonic visceral endoderm and sustains pluripotent cells in the epiblast before overt axial patterning. *Development.* 133:2497–2505.

Mesnard, D., M. Donnison, C. Fuerer, P.L. Pfeffer, and D.B. Constam. 2011. The microenvironment patterns the pluripotent mouse epiblast through paracrine Furin and Pace4 proteolytic activities. *Genes Dev.* 25:1871–1880. http://dx.doi.org/10.1101/gad.16738711

Miranda, L., J. Wolf, S. Pichuantes, R. Duke, and A. Franzusoff. 1996. Isolation of the human PC6 gene encoding the putative host protease for HIV-1 gp160 processing in $CD4^+$ T lymphocytes. *Proc. Natl. Acad. Sci. USA.* 93:7695–7700. http://dx.doi.org/10.1073/pnas.93.15.7695

Molloy, S.S., L. Thomas, J.K. VanSlyke, P.E. Stenberg, and G. Thomas. 1994. Intracellular trafficking and activation of the furin proprotein convertase: Localization to the TGN and recycling from the cell surface. *EMBO J.* 13:18–33.

Nelsen, S.M., and J.L. Christian. 2009. Site-specific cleavage of BMP4 by furin, PC6, and PC7. *J. Biol. Chem.* 284:27157–27166. http://dx.doi.org/10.1074/jbc.M109.028506

Nishioka, N., S. Yamamoto, H. Kiyonari, H. Sato, A. Sawada, M. Ota, K. Nakao, and H. Sasaki. 2008. *Tead4* is required for specification of trophectoderm in pre-implantation mouse embryos. *Mech. Dev.* 125:270–283. http://dx.doi.org/10.1016/j.mod.2007.11.002

Nishioka, N., K. Inoue, K. Adachi, H. Kiyonari, M. Ota, A. Ralston, N. Yabuta, S. Hirahara, R.O. Stephenson, N. Ogonuki, et al. 2009. The Hippo signaling pathway components Lats and Yap pattern Tead4 activity to distinguish mouse trophectoderm from inner cell mass. *Dev. Cell.* 16:398–410. http://dx.doi.org/10.1016/j.devcel.2009.02.003

Ozawa, M., and R. Kemler. 1990. Correct proteolytic cleavage is required for the cell adhesive function of uvomorulin. *J. Cell Biol.* 111:1645–1650. http://dx.doi.org/10.1083/jcb.111.4.1645

Pauken, C.M., and D.G. Capco. 2000. The expression and stage-specific localization of protein kinase C isotypes during mouse preimplantation development. *Dev. Biol.* 223:411–421. http://dx.doi.org/10.1006/dbio.2000.9763

Pey, R., C. Vial, G. Schatten, and M. Hafner. 1998. Increase of intracellular Ca^{2+} and relocation of E-cadherin during experimental decompaction of mouse embryos. *Proc. Natl. Acad. Sci. USA.* 95:12977–12982. http://dx.doi.org/10.1073/pnas.95.22.12977

Plachta, N., T. Bollenbach, S. Pease, S.E. Fraser, and P. Pantazis. 2011. Oct4 kinetics predict cell lineage patterning in the early mammalian embryo. *Nat. Cell Biol.* 13:117–123. http://dx.doi.org/10.1038/ncb2154

Plusa, B., S. Frankenberg, A. Chalmers, A.K. Hadjantonakis, C.A. Moore, N. Papalopulu, V.E. Papaioannou, D.M. Glover, and M. Zernicka-Goetz. 2005. Downregulation of Par3 and aPKC function directs cells towards the ICM in the preimplantation mouse embryo. *J. Cell Sci.* 118:505–515. http://dx.doi.org/10.1242/jcs.01666

Posthaus, H., C.M. Dubois, M.-H. Laprise, F. Grondin, M.M. Suter, and E. Müller. 1998. Proprotein cleavage of E-cadherin by furin in baculovirus over-expression system: Potential role of other convertases in

mammalian cells. *FEBS Lett.* 438:306–310. http://dx.doi.org/10.1016/S0014-5793(98)01330-1

Ralston, A., and J. Rossant. 2008. Cdx2 acts downstream of cell polarization to cell-autonomously promote trophectoderm fate in the early mouse embryo. *Dev. Biol.* 313:614–629. http://dx.doi.org/10.1016/j.ydbio.2007.10.054

Rayon, T., S. Menchero, A. Nieto, P. Xenopoulos, M. Crespo, K. Cockburn, S. Cañon, H. Sasaki, A.K. Hadjantonakis, J.L. de la Pompa, et al. 2014. Notch and hippo converge on *Cdx2* to specify the trophectoderm lineage in the mouse blastocyst. *Dev. Cell.* 30:410–422. http://dx.doi.org/10.1016/j.devcel.2014.06.019

Roebroek, A.J.M., L. Umans, I.G.L. Pauli, E.J. Robertson, F. van Leuven, W.J.M. Van de Ven, and D.B. Constam. 1998. Failure of ventral closure and axial rotation in embryos lacking the proprotein convertase Furin. *Development.* 125:4863–4876.

Rousselet, E., S. Benjannet, J. Hamelin, M. Canuel, and N.G. Seidah. 2011. The proprotein convertase PC7: Unique zymogen activation and trafficking pathways. *J. Biol. Chem.* 286:2728–2738. http://dx.doi.org/10.1074/jbc.M110.192344

Scamuffa, N., G. Siegfried, Y. Bontemps, L. Ma, A. Basak, G. Cherel, F. Calvo, N.G. Seidah, and A.M. Khatib. 2008. Selective inhibition of proprotein convertases represses the metastatic potential of human colorectal tumor cells. *J. Clin. Invest.* 118:352–363. http://dx.doi.org/10.1172/JCI32040

Seidah, N.G., and A. Prat. 2012. The biology and therapeutic targeting of the proprotein convertases. *Nat. Rev. Drug Discov.* 11:367–383. http://dx.doi.org/10.1038/nrd3699

Seidah, N.G., J. Hamelin, M. Mamarbachi, W. Dong, H. Tardos, M. Mbikay, M. Chretien, and R. Day. 1996. cDNA structure, tissue distribution, and chromosomal localization of rat PC7, a novel mammalian proprotein convertase closest to yeast kexin-like proteinases. *Proc. Natl. Acad. Sci. USA.* 93:3388–3393. http://dx.doi.org/10.1073/pnas.93.8.3388

Senturker, S., J.T. Thomas, J. Mateshaytis, and M. Moos Jr. 2012. A homolog of subtilisin-like proprotein convertase 7 is essential to anterior neural development in *Xenopus*. *PLoS ONE.* 7:e39380. http://dx.doi.org/10.1371/journal.pone.0039380

Spindle, A.I. 1978. Trophoblast regeneration by inner cell masses isolated from cultured mouse embryos. *J. Exp. Zool.* 203:483–489. http://dx.doi.org/10.1002/jez.1402030315

Stephenson, R.O., Y. Yamanaka, and J. Rossant. 2010. Disorganized epithelial polarity and excess trophectoderm cell fate in preimplantation embryos lacking E-cadherin. *Development.* 137:3383–3391. http://dx.doi.org/10.1242/dev.050195

Stephenson, R.O., J. Rossant, and P.P. Tam. 2012. Intercellular interactions, position, and polarity in establishing blastocyst cell lineages and embryonic axes. *Cold Spring Harb. Perspect. Biol.* 4:4. http://dx.doi.org/10.1101/cshperspect.a008235

Strumpf, D., C.A. Mao, Y. Yamanaka, A. Ralston, K. Chawengsaksophak, F. Beck, and J. Rossant. 2005. Cdx2 is required for correct cell fate specification and differentiation of trophectoderm in the mouse blastocyst. *Development.* 132:2093–2102. http://dx.doi.org/10.1242/dev.01801

Takahashi, S., T. Nakagawa, K. Kasai, T. Banno, S.J. Duguay, W.J. Van de Ven, K. Murakami, and K. Nakayama. 1995. A second mutant allele of furin in the processing-incompetent cell line, LoVo. Evidence for involvement of the homo B domain in autocatalytic activation. *J. Biol. Chem.* 270:26565–26569. http://dx.doi.org/10.1074/jbc.270.44.26565

Torres-Padilla, M.E., D.E. Parfitt, T. Kouzarides, and M. Zernicka-Goetz. 2007. Histone arginine methylation regulates pluripotency in the early mouse embryo. *Nature.* 445:214–218. http://dx.doi.org/10.1038/nature05458

Vestweber, D., A. Gossler, K. Boller, and R. Kemler. 1987. Expression and distribution of cell adhesion molecule uvomorulin in mouse preimplantation embryos. *Dev. Biol.* 124:451–456. http://dx.doi.org/10.1016/0012-1606(87)90498-2

Watanabe, T., J.S. Biggins, N.B. Tannan, and S. Srinivas. 2014. Limited predictive value of blastomere angle of division in trophectoderm and inner cell mass specification. *Development.* 141:2279–2288. http://dx.doi.org/10.1242/dev.103267

Wu, G., L. Gentile, T. Fuchikami, J. Sutter, K. Psathaki, T.C. Esteves, M.J. Araúzo-Bravo, C. Ortmeier, G. Verberk, K. Abe, and H.R. Schöler. 2010. Initiation of trophectoderm lineage specification in mouse embryos is independent of Cdx2. *Development.* 137:4159–4169. http://dx.doi.org/10.1242/dev.056630

Yagi, R., M.J. Kohn, I. Karavanova, K.J. Kaneko, D. Vullhorst, M.L. DePamphilis, and A. Buonanno. 2007. Transcription factor TEAD4 specifies the trophectoderm lineage at the beginning of mammalian development. *Development.* 134:3827–3836. http://dx.doi.org/10.1242/dev.010223

Yamanaka, Y., F. Lanner, and J. Rossant. 2010. FGF signal-dependent segregation of primitive endoderm and epiblast in the mouse blastocyst. *Development.* 137:715–724.

Ziomek, C.A., and M.H. Johnson. 1980. Cell surface interaction induces polarization of mouse 8-cell blastomeres at compaction. *Cell.* 21:935–942. http://dx.doi.org/10.1016/0092-8674(80)90457-2